Superexchange interactions in the two-dimensional $S = ½$ system $MV_3O_7$



2002 J. Phys.: Condens. Matter 14 5731

(http://iopscience.iop.org/0953-8984/14/23/307)

INSTITUTE OF PHYSICS PUBLISHING JOURNAL OF PHYSICS: CONDENSED MATTER

J. Phys.: Condens. Matter **14** (2002) 5731–5746 PII: S0953-8984(02)29525-9

# Superexchange interactions in the two-dimensional $S = \frac{1}{2}$ system $MV_3O_7$

**Noriaki Nishiguchi, Masashige Onoda[1] and Kenn Kubo[2]**

Institute of Physics, University of Tsukuba, Tennodai, Tsukuba 305-8571, Japan

Received 8 October 2001, in final form 8 February 2002
Published 30 May 2002
Online at stacks.iop.org/JPhysCM/14/5731

**Abstract**

The crystal structures and electronic properties of $MV_3O_7$ (M = Cd, Ca and Sr) and their mixed systems $Cd_{1-x}Ca_xV_3O_7$ and $Ca_{1-x}Sr_xV_3O_7$ have been explored by x-ray four-circle diffraction and through measurements of magnetization and electron paramagnetic resonance. The structure changes systematically according to the ionic radii of M. The analysis of susceptibility in terms of high-temperature series expansion of up to the eighth order indicates that the V–V exchange couplings sharing oxygen corners are antiferromagnetic and they are one order of magnitude larger than those sharing oxygen edges: one of the latter couplings is ferromagnetic and another coupling changes from ferromagnetic to antiferromagnetic depending on M. The transitions to the stripe phases for M = Ca and Sr are understood qualitatively. The magnitudes of the exchange couplings estimated here account for the spin-flop phenomena and their composition dependences are consistent with those of the V–V distances and V–O–V angles.

M This article features online multimedia enhancements

## 1. Introduction

Low-dimensional spin systems often show interesting phenomena due to quantum spin fluctuations. The $CaV_nO_{2n+1}$ system has a quasi-two-dimensional layer formed by the linkage of $V^{4+}O_5$ pyramids. $CaV_4O_9$ exhibits a spin gap [1] originating from weakly coupled plaquettes [2]. $CaV_2O_5$ ($n = 2$) also shows a gap [3], essentially due to corner sharing dimerization between the zigzag chains [3–9]. A slight substitution of $Na^+$ for $Ca^{2+}$ [10] and that of $Ti^{4+}$ for $V^{4+}$ [11] in $CaV_2O_5$ do not break this singlet bond. Although $MgV_2O_5$ has a layer similar to $CaV_2O_5$, the magnetic properties are significantly different. This is attributed to the difference of exchange couplings due to the structural distortion [4]. The exchange coupling for the inter-zigzag-chain path or for the rung path in a trellis layer in $MgV_2O_5$

[1] Author to whom any correspondence should be addressed.
[2] Present address: Department of Physics, Aoyama-Gakuin University, Chitosedai, Setagaya, Tokyo 157-8572, Japan.

  

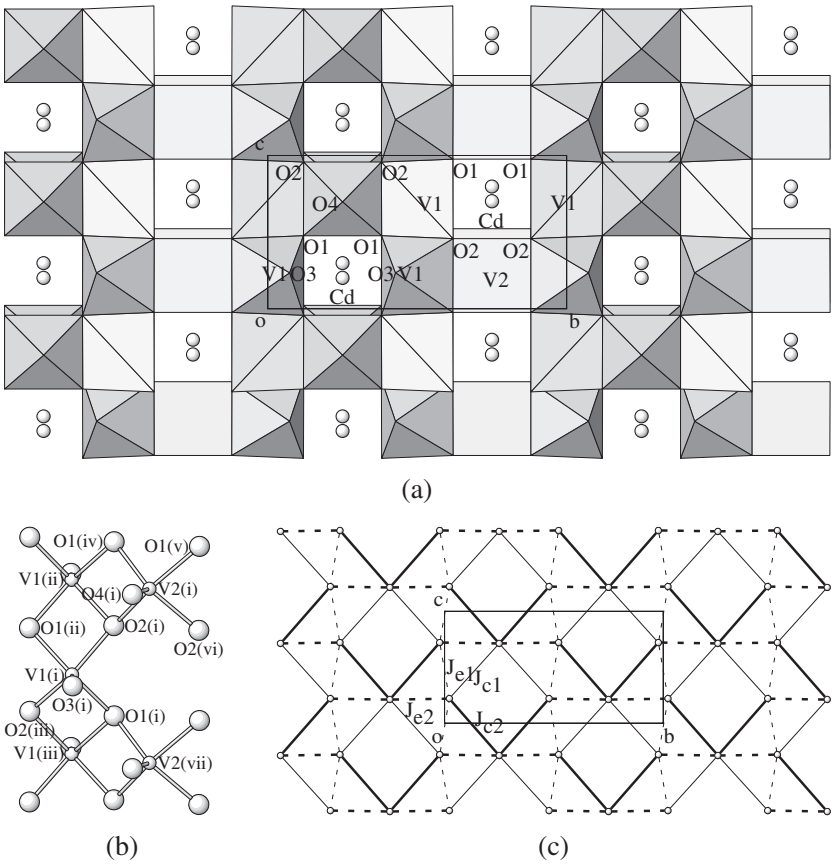


**Figure 1.** The crystal structure of $CdV_3O_7$ at 296 K: (a) the projection on the orthorhombic *bc*-plane with the polyhedral scheme; (b) the clinographic view of the V–O–V linkages with the translation codes listed in table 3 and (c) the two-dimensional spin network, where the dashed lines and the short full lines denote the edge-sharing V–V paths ($J_{e1}$ and $J_{e2}$) and the corner-sharing ones ($J_{c1}$ and $J_{c2}$) for the exchange couplings, respectively.

is smaller than that in $CaV_2O_5$, because of the smaller V–O–V angle and the larger V–O distance, which may enhance the low-dimensional properties [4] or incommensurate dynamic spin fluctuations [5]. Several experimental and theoretical studies support this idea [7–9]. While magnetic properties for the vanadium oxides with $V^{4+}O_5$ pyramids such as $MgVO_3$ [12][3], $LiV_2O_5$ [13], $CsV_2O_5$ [14], $[N(CH_3)_4]V_3O_7$, $(en)ZnV_6O_{14}$ and $(C_6H_{14}O_2)V_6O_{14}H_2O$ [15] are characterized by antiferromagnetic exchange couplings, $CdVO_3$ with a single zigzag-chain structure shows a ferromagnetic transition [16].

For the case of $n = 3$, there exist three isomorphous compounds: $MV_3O_7$ (M = Cd, Ca and Sr) [17][4]. The crystal structure of $CdV_3O_7$ determined precisely in this work as will be described later is displayed in figure 1(a) with the polyhedral scheme (space group *Pnma*). Cd ions are located between the $V_3O_7$ layers. On the basis of the V–O–V linkages shown in figure 1(b), two kinds of superexchange coupling constant sharing oxygen edges of the

[3] It is clearly indicated that $MgVO_3$ has an $S = 1/2$ one-dimensional chain with antiferromagnetic exchange coupling constant 124 K and an average *g*-factor 1.96.

[4] In this reference the space group *Pnam* is used for $CaV_3O_7$, while in the present work *Pnma* is adopted.

basal plane, $J_{e1}$ and $J_{e2}$, and those sharing oxygen corners, $J_{c1}$ and $J_{c2}$, are considered to be important to investigate magnetic properties of this system. The two-dimensional spin network with these exchange couplings is schematically shown in figure 1(c). On increasing the ionic radii of M, which are 1.03, 1.06 and 1.21 Å for Cd, Ca and Sr in the seven coordinations, respectively [18], the lattice constant of the $a$-axis perpendicular to the $V_3O_7$ layers increases significantly, but that of the $c$-axis varies little.

Electron paramagnetic resonance (EPR) measurements for the single crystals of $CaV_3O_7$ show that the $g$-factor is almost isotropic [19,20], indicating that this material should be treated as Heisenberg model,

$$H = \sum_{\langle i,j \rangle} J_{ij} \boldsymbol{S}_i \cdot \boldsymbol{S}_j, \tag{1}$$

where $\boldsymbol{S}_i$ is the spin operator at site $i$. The magnetic susceptibility of $CaV_3O_7$ has a maximum at around 90 K [21], which is characteristic of the low-dimensional system, and the long-range ordering to the stripe phase, the direction of magnetic moments being parallel to the $\boldsymbol{b}$-axis, occurs at around 24 K [22]. The modified spin-wave theory reveals this phase to be realized with $J_{c1} > 0.6932 J_{e1}$ under the simplified model of $J_{c1} = J_{c2}$ and $J_{e1} = J_{e2}$ [23].

The magnetic susceptibilities of $CdV_3O_7$ and $SrV_3O_7$ also have maxima at around 40 and 110 K, respectively [21]. The magnetization process of $SrV_3O_7$ at 15 K indicates the spin-flop transition. The neutron powder diffraction indicates this ordered phase to be the stripe type with magnetic moments parallel to the $\boldsymbol{a}$-axis [24]. In $CdV_3O_7$, on the other hand, no sign of the long-range order appears.

The difference of magnetic properties among these compounds may be attributed to the difference of exchange coupling constants, $J_{c1}$, $J_{c2}$, $J_{e1}$ and $J_{e2}$, shown in figure 1(c). The exchange couplings in $CaV_3O_7$ have been estimated using the LDA + $U$ method, but they do not account for the experimental data quantitatively [7]. In their paper, $J_{e2}$ is pointed out to be ferromagnetic. The net change in orbital energy has also been estimated from the spin-dimer analysis [25]. It roughly corresponds to the transfer integral between V ions, so that the antiferromagnetic exchange couplings may be deduced qualitatively with the negligible difference of the on-site repulsion energy for each site. However, in order to estimate the exchange couplings precisely, the ferromagnetic effects should be considered.

In this work, the mixed systems of $Cd_{1-x}Ca_xV_3O_7$ and $Ca_{1-x}Sr_xV_3O_7$ are prepared. In section 2, the lattice constants as a function of the composition are presented. In addition, the crystal structures of $CdV_3O_7$ and $Ca_{0.55}Sr_{0.45}V_3O_7$ determined precisely by means of the single-crystal diffraction are described with that of $CaV_3O_7$ redetermined for comparison among these atomic parameters. In section 3, the electronic properties revealed through measurements of magnetization and EPR are discussed, and the exchange coupling constants are estimated in detail in terms of high-temperature series expansion (HTSE). Section 4 is devoted to conclusions.

## 2. Crystal structures

### *2.1. Sample preparation and lattice constants*

The polycrystalline specimens of $Cd_{1-x}Ca_xV_3O_7$ were prepared by the solid-state reaction method. First, CaO and $V_2O_3$ were obtained by heating $CaCO_3$ (99.99% purity) at 1323 K in air and by heating $V_2O_5$ (99.99% purity) at 973 K in the atmosphere of $N_2/H_2$, respectively. The mixtures of $3V_2O_3$, $4x$CaO, $3V_2O_5$ and $4(1 - x)$CdO (99.99% purity) were pressed into pellets and heated at 973–1073 K in evacuated silica tubes for 24 h. For the Ca-doped specimens, grinding and heating were repeated several times in order to improve reaction. The

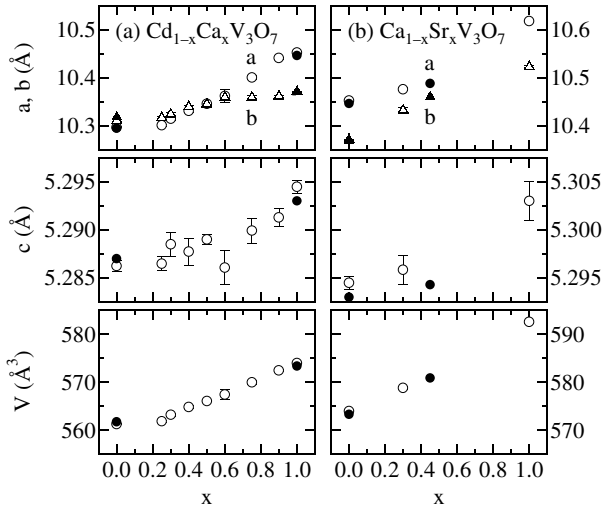


**Figure 2.** The composition dependence of the lattice constants of (a) $Cd_{1-x}Ca_xV_3O_7$ and (b) $Ca_{1-x}Sr_xV_3O_7$ systems. The full symbols represent the single-crystal diffraction results.

single crystals of $CdV_3O_7$ and $CaV_3O_7$ were prepared by the self-flux method at 1273 and 1323 K, respectively.

For the $Ca_{1-x}Sr_xV_3O_7$ system, $SrVO_3$ was first prepared by the method described in [26]. The mixtures of $4(1-x)$CaO, $4x$SrVO$_3$, $(3-x)V_2O_3$ and $(3-x)V_2O_5$ were pressed into pellets and heated at 1173 K in evacuated silica tubes for several days. The single crystals of $Ca_{1-x}Sr_xV_3O_7$ were prepared with a mixture of $SrV_3O_7$ and $CaV_3O_7$ by the self-flux method at 1293 K.

The specimens prepared above were confirmed to be single phase by x-ray powder diffraction with Cu K$\alpha$ at room temperature using a Rigaku RAD-IIC diffractometer. The lattice constants of $Cd_{1-x}Ca_xV_3O_7$ as a function of $x$ are shown in figure 2(a). Here, the full symbols indicate results for the single crystals as will be described below. For the region of $x \leqslant 0.25$ all of the lattice constants may be $x$ independent, but for $x > 0.25$ they increase linearly with $x$. This suggests that a certain kind of phase boundary exists at around $x = 0.25$. The lattice constants of $Ca_{1-x}Sr_xV_3O_7$ against $x$ are shown in figure 2(b). In this case, all of the parameters increase monotonically with increasing $x$, which is consistent with the previous result [17].

In order to consider the overall composition dependence of the lattice constants, the lattice constant ratios defined as $\Delta p = p/p_0 - 1$, where $p$ is the lattice constant and $p_0$ is that for $CaV_3O_7$, are plotted in figure 3 as a function of the ionic radius of the M ion, $r_M$, calculated for M = $Cd_{1-x}Ca_x$ and $Ca_{1-x}Sr_x$ with the data in [18]. It is clear that the change of the $c$-axis is small as compared with those of other parameters. In addition, the $r_M$-dependences of the $a$-axis and the volume $V$ for $r_M > 1.06$ Å ($=r_{Ca}$) are different from those for $r_M < 1.06$ Å. This behaviour does not appear for the $b$- and $c$-axes as guided by the dotted and full lines. The $x$-dependence of a magnetic coupling perpendicular to the $V_3O_7$ layer, $J_\perp$, in $Cd_{1-x}Ca_xV_3O_7$ is expected to be different from that in $Ca_{1-x}Sr_xV_3O_7$.

### *2.2. Structure determination*

The crystal structure of $CaV_3O_7$ was determined previously by single-crystal x-ray diffraction [17], and those of $CdV_3O_7$ and $SrV_3O_7$ were also determined by Rietveld

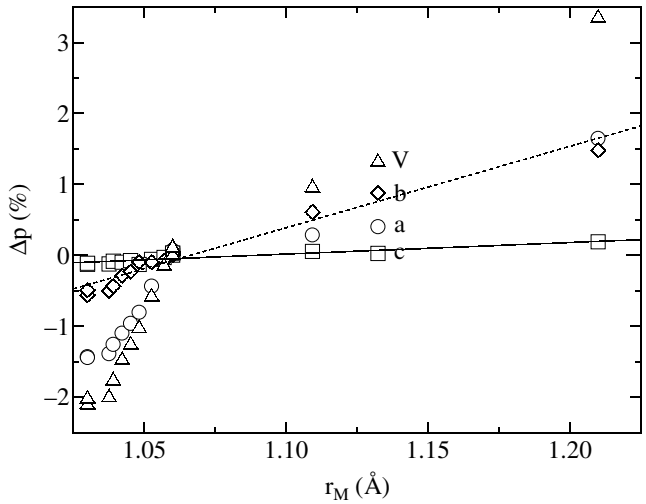


**Figure 3.** The ionic radius dependence of the lattice constant ratios of $Cd_{1-x}Ca_xV_3O_7$ and $Ca_{1-x}Sr_xV_3O_7$ systems, defined as $\Delta p = p/p_0 - 1$, where $p$ is the lattice constant and $p_0$ is that for $CaV_3O_7$. The dotted and full lines for the $b$- and $c$-axes are drawn as guides to the eye.

**Table 1.** The crystal data and a summary of the intensity measurements and refinements of $MV_3O_7$ (M = Cd, Ca and $Ca_{0.55}Sr_{0.45}$).

| | Cd | Ca | $Ca_{0.55}Sr_{0.45}$ |
|---|---|---|---|
| $a$ (Å) | 10.295(1) | 10.446(2) | 10.488(1) |
| $b$ (Å) | 10.3181(9) | 10.369(1) | 10.4604(8) |
| $c$ (Å) | 5.287(1) | 5.293(1) | 5.2943(6) |
| $V$ (Å$^3$) | 561.7(1) | 573.3(1) | 580.83(8) |
| $\mu_{\text{Mo K}\alpha}$ (mm$^{-1}$) | 8.555 | 5.657 | 13.777 |
| $D_{\text{cal}}$ (Mg m$^{-3}$) | 4.461 | 3.532 | 4.030 |
| $2\theta_{\max}$ | 120 | 120 | 90 |
| No of unique reflections | 4778 | 4871 | 2754 |
| $R_{\text{int}}$ | — | — | 0.075 |
| No of observations ($I > 3\sigma$) | 2552 | 2060 | 1250 |
| No of variables | 56 | 56 | 57 |
| $R$ | 0.047 | 0.051 | 0.044 |
| $R_{\text{w}}$ | 0.043 | 0.045 | 0.035 |

analysis [21]. In this work, the detailed structures of $CdV_3O_7$ and $Ca_{0.55}Sr_{0.45}V_3O_7$ are determined at 296 and 297 K, respectively, by means of x-ray four-circle diffraction using a Rigaku AFC-7R diffractometer (custom made) with graphite monochromated Mo K$\alpha$ radiation. The structure result for $CaV_3O_7$ at 295 K is also presented to allow us to explore the composition dependence of the atomic parameters.

Intensity data for the structure analysis were collected using the $\omega$–$2\theta$ scan technique and corrections for Lorentz polarization, absorption and secondary extinction effects were applied. For all of the compounds, the space group and the $Z$-value were determined to be $Pnma$ (No 62) and $Z = 4$. The lattice constants and the various parameters used for the structure refinements are summarized in table 1.

All of the structures were solved by direct methods [27], expanded using Fourier techniques, and refined by full-matrix least-squares calculations with anisotropic displacement

**Table 2.** Atomic coordinates and equivalent isotropic thermal parameters $B_{eq}$ (Å$^2$) of $MV_3O_7$ (M = Cd, Ca and $Ca_{0.55}Sr_{0.45}$) at room temperature.

| Atom | | Cd | Ca | $Ca_{0.55}Sr_{0.45}$ |
|---|---|---|---|---|
| V1 | $x$ | 0.31421(5) | 0.31243(4) | 0.31184(6) |
| | $y$ | 0.02195(4) | 0.02041(4) | 0.01735(5) |
| | $z$ | 0.27973(9) | 0.28326(9) | 0.2647(1) |
| | $B_{eq}$ | 0.492(5) | 0.477(5) | 0.651(9) |
| V2 | $x$ | 0.28707(7) | 0.28858(6) | 0.29301(9) |
| | $y$ | $\frac{1}{4}$ | $\frac{1}{4}$ | $\frac{1}{4}$ |
| | $z$ | 0.7876(1) | 0.7921(1) | 0.7690(2) |
| | $B_{eq}$ | 0.498(7) | 0.465(7) | 0.64(1) |
| M | $x$ | 0.08528(3) | 0.08455(8) | 0.07790(8) |
| | $y$ | $\frac{1}{4}$ | $\frac{1}{4}$ | $\frac{1}{4}$ |
| | $z$ | 0.29777(7) | 0.2996(2) | 0.2718(2) |
| | $B_{eq}$ | 0.727(4) | 0.649(10) | 0.95(1) |
| O1 | $x$ | 0.2190(2) | 0.2202(2) | 0.2261(3) |
| | $y$ | 0.1194(2) | 0.1202(2) | 0.1207(3) |
| | $z$ | 0.0231(4) | 0.0257(4) | 0.0058(4) |
| | $B_{eq}$ | 0.63(3) | 0.58(3) | 0.71(5) |
| O2 | $x$ | 0.2236(2) | 0.2259(2) | 0.2298(3) |
| | $y$ | 0.1198(2) | 0.1202(2) | 0.1209(3) |
| | $z$ | 0.5423(4) | 0.5477(4) | 0.5270(4) |
| | $B_{eq}$ | 0.61(3) | 0.63(3) | 0.71(5) |
| O3 | $x$ | 0.4623(2) | 0.4597(2) | 0.4609(3) |
| | $y$ | 0.0729(3) | 0.0659(2) | 0.0546(3) |
| | $z$ | 0.2657(5) | 0.2666(5) | 0.2557(6) |
| | $B_{eq}$ | 1.11(4) | 1.11(4) | 1.42(5) |
| O4 | $x$ | 0.4440(4) | 0.4440(3) | 0.4481(4) |
| | $y$ | $\frac{1}{4}$ | $\frac{1}{4}$ | $\frac{1}{4}$ |
| | $z$ | 0.8031(8) | 0.8082(7) | 0.7772(9) |
| | $B_{eq}$ | 1.16(5) | 1.09(5) | 1.45(8) |

parameters. The atomic scattering factors were taken from [28], and anomalous dispersion effects were included with the values given by [29]. The residual factors defined as

$$R = \left[\sum(|F_o| - |F_c|)^2\right] \Big/ \left(\sum |F_o|\right) \tag{2}$$

and

$$R_w = \left\{\left[\sum w(|F_o| - |F_c|)^2\right] \Big/ \left(\sum w F_o^2\right)\right\}^{1/2}, \tag{3}$$

where $|F_o|$ and $|F_c|$ are an observed structure factor and a calculated one, respectively, are finally as listed in table 1[5]. All of the calculations were performed using the teXsan crystallographic software package [30].

The atomic coordinates and the equivalent isotropic thermal parameters are listed in table 2. The selected interatomic distances and angles, and the V valences estimated on the basis of the bond-length–bond-strength relation [31], are listed in table 3. As shown in figures 1(a) and (b), the structure is expressed in terms of $V^{4+}O_5$ pyramids which are linked by sharing edges and corners to form a quasi-two-dimensional $V_3O_7$ layer. The V ions occupy two crystallographically independent sites, V1 and V2. The $V1O_5$ pyramids are tilted significantly

[5] Supplementary data files are available from the paper's abstract page in the online journal; see http://www.iop.org.

**Table 3.** Interatomic distances (Å), angles (degrees) and V valences of $MV_3O_7$ (M = Cd, Ca and $Ca_{0.55}Sr_{0.45}$) at room temperature, where the translation codes are (i) $x, y, z$; (ii) $\frac{1}{2} - x, -y, \frac{1}{2} + z$; (iii) $\frac{1}{2} - x, -y, -\frac{1}{2} + z$; (iv) $x, y, 1 + z$; (v) $x, \frac{1}{2} - y, 1 + z$; (vi) $x, \frac{1}{2} - y, z$; (vii) $x, y, -1 + z$; (viii) $-\frac{1}{2} + x, \frac{1}{2} - y, \frac{1}{2} - z$; (ix) $-\frac{1}{2} + x, y, \frac{1}{2} - z$ and (x) $-\frac{1}{2} + x, \frac{1}{2} - y, \frac{3}{2} - z$.

| | Cd | Ca | $Ca_{0.55}Sr_{0.45}$ |
|---|---|---|---|
| V1(i)–O1(i) | 1.953(2) | 1.964(2) | 1.963(3) |
| V1(i)–O1(ii) | 1.975(2) | 1.972(2) | 1.968(3) |
| V1(i)–O2(i) | 1.954(2) | 1.961(2) | 1.960(3) |
| V1(i)–O2(iii) | 1.967(2) | 1.959(2) | 1.966(3) |
| V1(i)–O3(i) | 1.614(3) | 1.612(2) | 1.612(2) |
| O1(i)–O2(i) | 2.746(3) | 2.764(3) | 2.760(3) |
| O1(i)–O2(iii) | 2.540(3) | 2.558(2) | 2.572(3) |
| O1(i)–O3(i) | 2.854(3) | 2.864(3) | 2.879(4) |
| O1(ii)–O2(i) | 2.540(3) | 2.558(2) | 2.572(3) |
| O1(ii)–O2(iii) | 2.542(3) | 2.530(3) | 2.535(3) |
| O1(ii)–O3(i) | 3.045(3) | 3.023(3) | 2.993(4) |
| O2(i)–O3(i) | 2.900(4) | 2.915(3) | 2.902(4) |
| O2(iii)–O3(i) | 3.002(3) | 2.971(3) | 2.973(4) |
| V2(i)–O1(iv, v) | 1.964(2) | 1.962(2) | 1.973(3) |
| V2(i)–O2(i, vi) | 1.978(2) | 1.978(2) | 1.976(3) |
| V2(i)–O4(i) | 1.618(4) | 1.626(4) | 1.627(4) |
| O1(iv)–O1(v) | 2.695(4) | 2.691(4) | 2.706(7) |
| O1(iv)–O2(i) | 2.542(3) | 2.530(3) | 2.535(3) |
| O1(iv,v)–O2(vi) | 2.921(4) | 2.932(4) | 2.952(5) |
| O1(v)–O2(vi) | 2.542(3) | 2.530(3) | 2.535(3) |
| O2(i)–O2(vi) | 2.686(4) | 2.692(4) | 2.700(7) |
| O2(i,vi)–O4(i) | 2.976(4) | 2.984(4) | 2.970(5) |
| V1(i)–V1(ii, iii) | 2.9904(4) | 2.9807(4) | 2.9701(6) |
| V1(i)–V2(iii) | 2.9937(6) | 2.9963(5) | 3.0051(7) |
| V1(i)–V2(vii) | 3.5193(7) | 3.5338(7) | 3.585(1) |
| V1(i)–V2(i) | 3.5814(7) | 3.6034(7) | 3.618(1) |
| V1(i)–O1(i)–V1(iii) | 99.17(10) | 98.43(9) | 98.1(1) |
| V1(i)–O2(i)–V1(ii) | 99.41(9) | 98.97(10) | 98.3(1) |
| V1(iii)–O1(i)–V2(vii) | 98.95(10) | 99.22(9) | 99.4(1) |
| V1(ii)–O2(i)–V2(i) | 98.73(9) | 99.09(9) | 99.3(1) |
| V1(i)–O1(i)–V2(vii) | 128.0(1) | 128.4(1) | 131.2(2) |
| V1(i)–O2(i)–V2(i) | 131.2(1) | 132.3(1) | 133.6(2) |
| M(i)–O1(i, vi) | 2.413(2) | 2.434(2) | 2.496(3) |
| M(i)–O2(i, vi) | 2.346(2) | 2.391(2) | 2.487(3) |
| M(i)–O3(viii, ix) | 2.249(3) | 2.338(2) | 2.389(3) |
| M(i)–O4(x) | 2.563(4) | 2.542(4) | 2.749(5) |
| V1 valence | 4.07 | 4.07 | 4.06 |
| V2 valence | 3.98 | 3.95 | 3.91 |

from the *bc*-plane, and the tilting angle varies greatly depending on the M ions. The M ions are located between the $V_3O_7$ layers.

The atomic coordinates of $CaV_3O_7$ determined here are almost consistent with those by Bouloux and Galy except for the O4 site. Due to differences of this and the lattice constants, the distances between V and the apical O ions are larger than the previous values. The V1(i)–O3(i) (V2(i)–O4(i)) distance is 1.612 (1.626) Å, while the previous value is 1.593 (1.570) Å. For all of the atomic coordinates of $CdV_3O_7$, our results are not consistent with the previous results. Significant differences are found for $y$ of V2, $y$ of O2 and $x$ of O1. Due to the differences in the atomic coordinates and the lattice constants, the absolute differences for the distances

**Table 4.** The main parts of the ground-state wavefunctions of $3d^1$ for the $VO_5$ pyramid of $MV_3O_7$ (M = Cd, Ca and $Ca_{0.55}Sr_{0.45}$) calculated with the Hartree–Fock function from a crystal field, where $\boldsymbol{x} \parallel \boldsymbol{c}$ and $\boldsymbol{z} \parallel \boldsymbol{a}$.

| M | V1 | V2 |
|---|---|---|
| Cd | $0.839d_{x^2-y^2} - 0.513d_{zx} + 0.162d_{3z^2-r^2}$ | $0.990d_{x^2-y^2} + 0.115d_{yz} + 0.084d_{3z^2-r^2}$ |
| Ca | $0.856d_{x^2-y^2} - 0.489d_{zx} + 0.137d_{3z^2-r^2}$ | $0.990d_{x^2-y^2} + 0.105d_{yz} + 0.094d_{3z^2-r^2}$ |
| $Ca_{0.55}Sr_{0.45}$ | $0.888d_{x^2-y^2} - 0.445d_{zx} + 0.100d_{3z^2-r^2}$ | $0.993d_{x^2-y^2} + 0.054d_{yz} + 0.104d_{3z^2-r^2}$ |

of V1(i)–O1(i), V1(i)–O2(i), V1(i)–O2(iii), V1(i)–O3(i) and V2(i)-O2(i, vi) are larger than 0.02 Å, and those for the angles of V1(i)–O1(i)–V1(iii), V1(i)–O1(i)–V2(vii), V1(i)–O2(i)–V2(i) and V1(ii)–O2(i)–V2(i) are larger than 1°. Moreover, in this work, the thermal parameters of O for $CdV_3O_7$ are larger than those of V, which contrasts with the previous results.

The atomic coordinates of $SrV_3O_7$ reported previously are out from the extrapolated values based on our results. Here, the distances of V1(i)–V1(ii, iii) and V1(i)–V2(vii) and the angles of V1(i)–O1(i)–V1(iii), V1(i)–O1(i)–V2(vii), V1(iii)–O1(i)–V2(vii) and V1(i)–O2(i)–V1(ii) of $SrV_3O_7$ deviate significantly from the tendency for $CdV_3O_7$, $CaV_3O_7$ and $Ca_{0.55}Sr_{0.45}V_3O_7$.

The bond-lengths and bond-angles of $V^{4+}O_5$ pyramids vary systematically with the ionic radii of M. In contrast, the previous work indicates that for the composition of $CaV_3O_7$, the distance of V1(i)–V1(ii, iii) along the *c*-axis and the angles of V1(iii)–O1(i)–V2(vii), V1(ii)–O2(i)–V2(i) and V1(i)–O2(i)–V2(i) indicate a minimum, and the distance of V1(i)–V2(vii) and the angle of V1(i)–O1(i)–V2(vii) show a maximum.

The ground-state wavefunction of the 3d electron of $V^{4+}$ is calculated with the Hartree–Fock function from a crystal field of the nearest five oxygens. The results are shown in table 4, where the $\boldsymbol{x}$- and $\boldsymbol{z}$-axes correspond to the $\boldsymbol{c}$- and $\boldsymbol{a}$-axes, respectively. All of the compounds have similar states. The ground state for V1 is a hybrid orbital like $d_{x^2-y^2}$ rotating around the *x*-axis with angles of 18.35, 16.95 and 14.70° for $CdV_3O_7$, $CaV_3O_7$ and $Ca_{0.55}Sr_{0.45}V_3O_7$, respectively. This angle corresponds to that between the *z*-axis and the direction of V1(i)–O3(i). On the other hand, the ground state of V2 is almost $d_{x^2-y^2}$.

The magnetic susceptibility of $MV_3O_7$ shows a broad maximum at certain temperatures $T_{\chi\max}$, which increases with increasing ionic radii of M as will be described in section 3.1. Since $T_{\chi\max}$ is related to the exchange coupling constants, the systematic change of the structure stated above is reasonable.

## 3. Electronic properties

### *3.1. Magnetization*

The magnetizations with a field of up to 1 T for the polycrystalline specimens were measured by the Faraday method at temperatures between 4.2 and 800 K. The magnetic susceptibility $\chi$ was deduced from the linear part of the magnetization–field ($M$–$H$) curve. The temperature dependence of $\chi$ for $Cd_{1-x}Ca_xV_3O_7$ and $Ca_{1-x}Sr_xV_3O_7$ is shown in figure 4(a). For all of the specimens, $\chi$ at high temperatures is explained by considering the contributions of the Curie–Weiss-type susceptibility $\chi_{CW}$ and the temperature-independent susceptibility of the Van Vleck orbital and diamagnetic components, $\chi_0$:

$$\chi = \chi_{CW} + \chi_0, \tag{4}$$

$$\chi_{CW} = \frac{C}{T + T_W}, \tag{5}$$

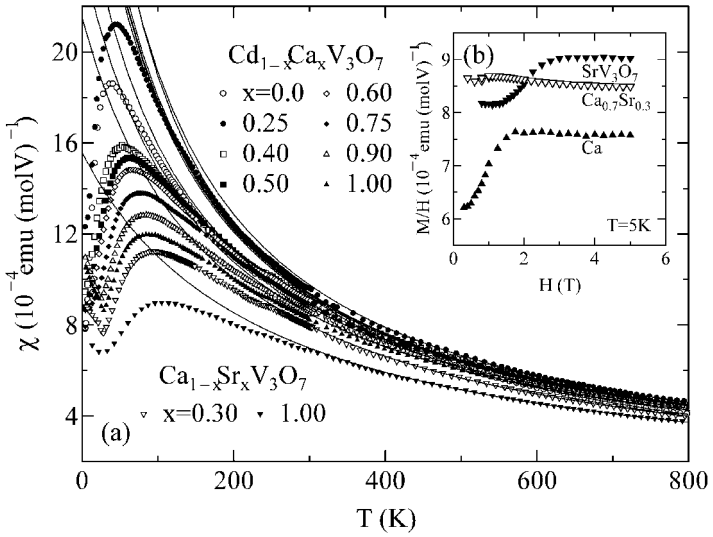


**Figure 4.** (a) The temperature dependence of the magnetic susceptibility $\chi$ of $Cd_{1-x}Ca_xV_3O_7$ and $Ca_{1-x}Sr_xV_3O_7$, where the full curves indicate the results calculated on the basis of the Curie–Weiss law; (b) the field dependence of the susceptibility $M/H$ for $CaV_3O_7$, $Ca_{0.7}Sr_{0.3}V_3O_7$ and $SrV_3O_7$ at 5 K.

**Table 5.** The parameters of the Curie–Weiss law for $MV_3O_7$; the Curie constant $C$ (emu K (mol V)$^{-1}$), the Weiss temperature $T_W$ (K) and the temperature-independent susceptibility $\chi_0$ ($10^{-5}$ emu (mol V)$^{-1}$).

| M | $C$ | $T_W$ | $\chi_0$ |
|---|---|---|---|
| Cd | 0.358 | 89.5 | 0.49 |
| $Cd_{0.75}Ca_{0.25}$ | 0.367 | 97.3 | 5.22 |
| $Cd_{0.60}Ca_{0.40}$ | 0.362 | 108.5 | 4.78 |
| $Cd_{0.50}Ca_{0.50}$ | 0.361 | 111.4 | 4.77 |
| $Cd_{0.40}Ca_{0.60}$ | 0.362 | 106.5 | 4.85 |
| $Cd_{0.25}Ca_{0.75}$ | 0.357 | 107.6 | 5.81 |
| $Cd_{0.10}Ca_{0.90}$ | 0.363 | 135.0 | 4.64 |
| Ca | 0.365 | 153.4 | 4.52 |
| $Ca_{0.70}Sr_{0.30}$ | 0.365 | 171.7 | 2.40 |
| Sr | 0.362 | 235.8 | 2.37 |

where $C$ and $T_W$ are the Curie constant and the Weiss temperature, respectively. The full curves in figure 4(a) are drawn on the basis of the parameters listed in table 5. Since the $V^{4+}$ ions have the average $g$-factor of 1.97 as will be described in section 3.2, the Curie constants listed here are consistent with the values expected from a model where all of the V ions are tetravalent. As found in table 5, $T_W$ increases on increasing the ionic radii of M.

For $Cd_{1-x}Ca_xV_3O_7$, the compounds with $x = 0.9$ and 1 indicate the magnetic transitions at $T_c = 25$ and 27 K, respectively, below which the spin-flop phenomena appear. All of the data show a broad maximum at a certain temperature $T_{\chi max}$, which increases with increasing $x$. The compound with $x = 0.25$ has the largest susceptibility.

For $Ca_{1-x}Sr_xV_3O_7$, $\chi$ for $x = 0.30$ exhibits a maximum at 95 K and a sharp minimum at 27 K, which is similar to the case for $CaV_3O_7$. Thus, the transition is expected to occur at 27 K. In $SrV_3O_7$, a susceptibility maximum appears at 107 K, but a sharp minimum does

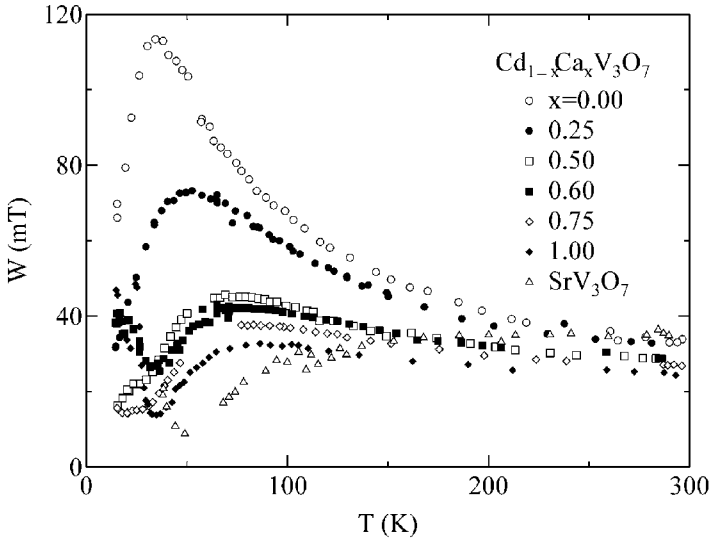


**Figure 5.** The temperature dependence of the EPR linewidth $W$ of $Cd_{1-x}Ca_xV_3O_7$ and $SrV_3O_7$.

not. The magnetization process at 5 K of this compound behaves like an antiferromagnetic material as described later.

The magnetization process at a field of up to 5 T was measured for $SrV_3O_7$, $Ca_{0.7}Sr_{0.3}V_3O_7$ and $Cd_{1-x}Ca_xV_3O_7$ with $x = 1, 0.75, 0.5, 0.25$ and 0 at 5 K by means of a SQUID. As shown in figure 4(b), for $CaV_3O_7$ and $SrV_3O_7$, $M/H$-values increase as $H$ increases, and saturate at 2 and 2.5 T, respectively, indicating a spin-flop. Other compounds do not show such a behaviour. It should be noted that $Ca_{0.7}Sr_{0.3}V_3O_7$ does not show the spin-flop, although the sharp minimum of susceptibility exists.

### *3.2. Electron paramagnetic resonance*

The EPR measurements for the polycrystalline specimens of $Cd_{1-x}Ca_xV_3O_7$ with $x = 0$, 0.25, 0.5, 0.6, 0.75 and 1 were performed using a JEOL X-band spectrometer at temperatures between 15 and 300 K. All of the compounds show a single Lorentzian with $g \simeq 1.97$ at room temperatures. The temperature dependence of the peak-to-peak linewidth of absorption derivative, $W$, is shown in figure 5, where $g$ is temperature independent. For all of the compounds, $W$ exhibits a maximum at a certain temperature. Below 60 K, the spectra for $x = 0.25, 0.5$ and 0.6 seem to be expressed as a superposition of two Lorentzians with large and small linewidths. Their temperature dependences are similar to those of $CdV_3O_7$ and $CaV_3O_7$, and the intensity ratio of the signal with the small linewidth increases with increasing $x$. This suggests that the electronic phases similar to those of $CdV_3O_7$ and $CaV_3O_7$ are segregated in the mixed system at temperatures below 60 K. In order to clarify this anomalous result, further investigations are necessary. For other compounds, the temperature at which $W$ indicates a maximum agrees with $T_{\chi\max}$. In $CaV_3O_7$, $W$ increases again below 32 K and diverges at around 25 K. This is due to the magnetic transition. The spectra for the polycrystalline specimens of $SrV_3O_7$ also exhibit a single Lorentzian with $g \simeq 1.97$. As shown in figure 5, $W$ is temperature independent above 180 K, below which it decreases with decreasing temperature, and then takes a minimum at around 50 K and finally diverges at 40 K. This result suggests the occurrence of the magnetic transition.

**Table 6.** Some of the coefficients of equation (6), $a_{\{n_I\}}$, calculated on the basis of the high-temperature series expansion for the $MV_3O_7$ system, where $\{n_I\} = (i, j, k, l)$; this corresponds to the term of $J_{e1}^i J_{e2}^j J_{c1}^k J_{c2}^l / T^{i+j+k+l}$.

| $(i, j, k, l)$ | $a_{\{n_I\}}$ | $(i, j, k, l)$ | $a_{\{n_I\}}$ | $(i, j, k, l)$ | $a_{\{n_I\}}$ |
|---|---|---|---|---|---|
| (0, 0, 0, 0) | 3 | (1, 0, 2, 0) | −0.062 5 | (1, 2, 1, 0) | −0.015 625 |
| | | (1, 0, 1, 1) | −0.062 5 | (1, 2, 0, 1) | −0.015 625 |
| (1, 0, 0, 0) | −1 | (1, 0, 0, 2) | −0.062 5 | (1, 1, 2, 0) | −0.015 625 |
| (0, 1, 0, 0) | −1 | (0, 3, 0, 0) | 0.083 333 333 | (1, 1, 1, 1) | 0.333 333 33 |
| (0, 0, 1, 0) | −1 | (0, 2, 1, 0) | 0 | (1, 1, 0, 2) | −0.015 625 |
| (0, 0, 0, 1) | −1 | (0, 2, 0, 1) | 0 | (1, 0, 3, 0) | −0.052 083 333 |
| | | (0, 1, 2, 0) | 0 | (1, 0, 2, 1) | 0.114 583 33 |
| (2, 0, 0, 0) | 0 | (0, 1, 1, 1) | −0.75 | (1, 0, 1, 2) | 0.114 583 33 |
| (1, 1, 0, 0) | 0.5 | (0, 1, 0, 2) | 0 | (1, 0, 0, 3) | −0.052 083 333 |
| (1, 0, 1, 0) | 0.5 | (0, 0, 3, 0) | 0.083 333 333 | (0, 4, 0, 0) | 0.036 458 333 |
| (1, 0, 0, 1) | 0.5 | (0, 0, 2, 1) | 0 | (0, 3, 1, 0) | −0.088 541 666 |
| (0, 2, 0, 0) | −0.125 | (0, 0, 1, 2) | 0 | (0, 3, 0, 1) | −0.088 541 666 |
| (0, 1, 1, 0) | 0.75 | (0, 0, 0, 3) | 0.083 333 333 | (0, 2, 2, 0) | 0.145 833 33 |
| (0, 1, 0, 1) | 0.75 | | | (0, 2, 1, 1) | 0.057 291 666 |
| (0, 0, 2, 0) | −0.125 | (4, 0, 0, 0) | 0.026 041 666 | (0, 2, 0, 2) | 0.145 833 33 |
| (0, 0, 1, 1) | 0.75 | (3, 1, 0, 0) | −0.041 666 666 | (0, 1, 3, 0) | −0.088 541 666 |
| (0, 0, 0, 2) | −0.125 | (3, 0, 1, 0) | −0.041 666 666 | (0, 1, 2, 1) | 0.161 458 33 |
| | | (3, 0, 0, 1) | −0.041 666 666 | (0, 1, 1, 2) | 0.161 458 33 |
| (3, 0, 0, 0) | 0.083 333 333 | (2, 2, 0, 0) | 0.062 5 | (0, 1, 0, 3) | −0.088 541 666 |
| (2, 1, 0, 0) | 0 | (2, 1, 1, 0) | −0.005 208 3333 | (0, 0, 4, 0) | 0.036 458 333 |
| (2, 0, 1, 0) | 0 | (2, 1, 0, 1) | −0.005 208 3333 | (0, 0, 3, 1) | −0.088 541 666 |
| (2, 0, 0, 1) | 0 | (2, 0, 2, 0) | 0.062 5 | (0, 0, 2, 2) | 0.093 75 |
| (1, 2, 0, 0) | −0.062 5 | (2, 0, 1, 1) | 0.020 833 333 | (0, 0, 1, 3) | −0.088 541 666 |
| (1, 1, 1, 0) | −0.312 5 | (2, 0, 0, 2) | 0.062 5 | (0, 0, 0, 4) | 0.036 458 333 |
| (1, 1, 0, 1) | −0.312 5 | (1, 3, 0, 0) | −0.052 083 333 | | |

### *3.3. High-temperature series expansion*

In order to estimate the exchange coupling constants, the magnetic susceptibility is fitted in terms of HTSE as follows:

$$\chi = \frac{C}{T} \sum_{n}^{8} \sum_{\sum n_I = n} \frac{a_{\{n_I\}}}{3} \prod_I \left( \frac{J_I}{T} \right)^{n_I} + \chi_0, \tag{6}$$

where $C = 0.363$ emu K (mol V)$^{-1}$ with the use of the EPR $g$-factor measured; $\Pi_I$ is a multiplication taken over $I =$ e1, e2, c1 and c2 shown in figure 1(c) and $a_{\{n_I\}}$ is a coefficient for $\{n_I\} = (n_{e1}, n_{e2}, n_{c1}, n_{c2})$ determined for the spin network. Some of the values are listed in table 6[4], where $(i, j, k, l)$ corresponds to the term of $J_{e1}^i J_{e2}^j J_{c1}^k J_{c2}^l / T^{i+j+k+l}$.

Because the HTSE analysis is valid only at high temperatures, the temperature region for the analysis should be taken into consideration precisely. The lower temperature limit $T_{min}$ ranges from 2.2 to 2.3 times as large as the effective exchange coupling constant $J_{eff}$ estimated on the basis of the coefficients of equation (6) as described in appendix A. Since the fit by equation (6) does not converge owing to the number of parameters, $\chi_0$ is fixed to the value estimated on the basis of Curie–Weiss law as listed in table 5. In addition, $J_{c1}$ is assumed to be equal to $J_{c2}$ for the following reason. Their difference corresponds to that between the superexchange couplings along the paths of V1(i)–O1(i)–V2(vii) and V1(i)–O2(i)–V2(i).

[4] A full table is described in supplementary data files.

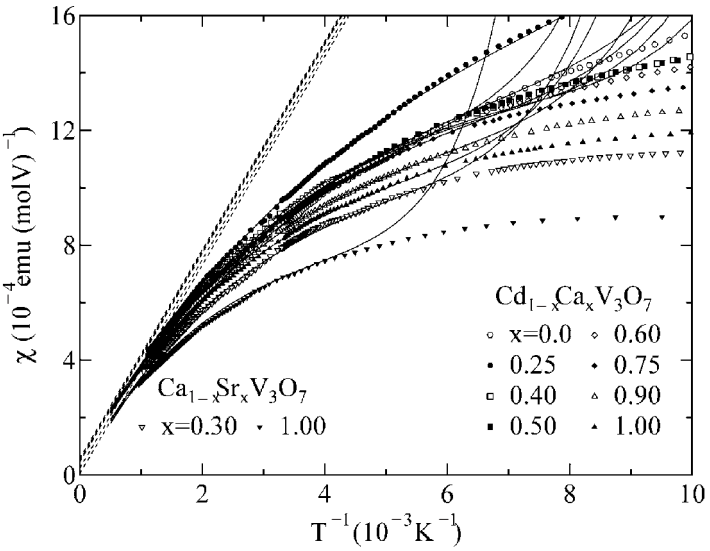


**Figure 6.** The magnetic susceptibility $\chi$ against the inverse temperature of $Cd_{1-x}Ca_xV_3O_7$ and $Ca_{1-x}Sr_xV_3O_7$ compared with the HTSE results of up to the eighth order (full curves). The dotted lines indicate the temperature dependence of the Curie law.

Here, the V2(i)–O1(iv) bond-length is 0.014 Å smaller than that of the V2(i)–O2(i) path, while the angle of V1(i)–O2(i)–V2(i) is closer to 180° than that of V1(i)–O1(i)–V2(vii). The former difference provides a superexchange coupling constant of the V1(i)–O1(i)–V2(vii) path larger than that of the V1(i)–O2(i)–V2(i) path, but the latter difference gives the inverse effect. In effects when $J_{c1}$ and $J_{c2}$ are treated without the constraint, their difference is found to be small.

A comparison between the experimental and calculated results as a function of $T^{-1}$ is shown in figure 6. The composition dependence of the exchange couplings is shown in figure 7, where negative $J_I$ means ferromagnetic coupling, and the error bars are estimated from the dispersion of the experimental data. $J_c$ ($=J_{c1} = J_{c2}$) is significantly larger than the absolute values of $J_{e1}$ and $J_{e2}$, and it increases with the increase of the ionic radii of M. $J_{e1}$ changes from ferromagnetic ($CdV_3O_7$) to antiferromagnetic, while $J_{e2}$ is always smaller than zero (ferromagnetic). When $J_{e1}$ is antiferromagnetic, the two-dimensional network without frustration is formed, which allows a magnetic transition to occur. This is the case for $CaV_3O_7$ and $SrV_3O_7$. The composition $Cd_{0.25}Ca_{0.75}V_3O_7$ has $J_{e1}$ and $J_{e2}$ close to zero, so that the spin network would be approximated as a one-dimensional system, two $S = \frac{1}{2}$ and one $S = \frac{1}{2}$ alternating on a chain with antiferromagnetic exchange coupling. In this case, a ferrimagnetic state should appear as found on the basis of the Marshall–Lieb–Mattis theorem [32, 33], and this has recently been investigated in detail [34]. In contrast, in $Cd_{0.25}Ca_{0.75}V_3O_7$, a divergent behaviour of $\chi$ or a remanent magnetization does not appear at low temperatures. The origin of this discrepancy should be clarified in the future.

For $CdV_3O_7$, $J_{e2}$ is $-100$ K and $J_{e1}$ is very small, so the long-range-ordered phase similar to the stripe type is expected to be formed. However, this compound has no magnetic transition at temperatures above 5 K. Therefore, it is expected that the coupling perpendicular to the $V_3O_7$ layer ($J_\perp$) plays an essential role. From the crystal structures described before, the most effective path for $J_\perp$ is considered to correspond to V1(i)–O3(i)–V1($1 - x$, $-y$, $1 - z$); for M = Cd, Ca and $Ca_{0.55}Sr_{0.45}$, the V1–V1 distance and the V1–O3–V1 angle range from 4.50 to 4.68 Å and from 120.2° to 125.2°, respectively. A reduction of $J_\perp$ due to the decrease of the

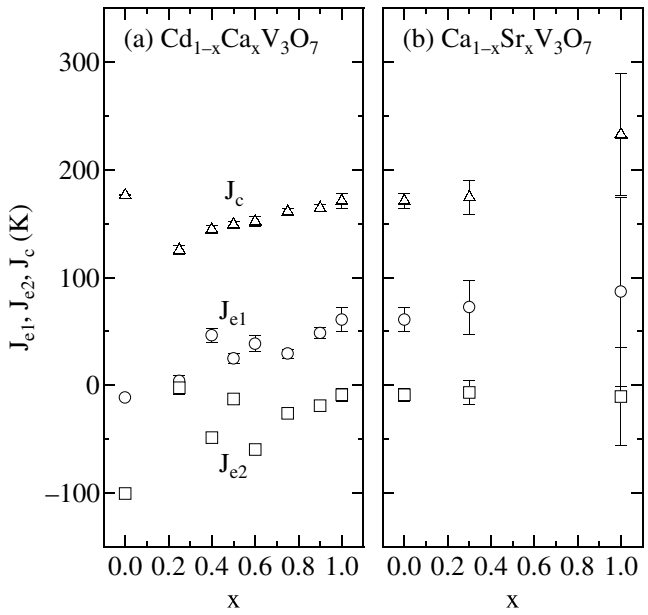


**Figure 7.** The composition dependence of the exchange coupling constants $J_c$, $J_{e1}$ and $J_{e2}$ for $Cd_{1-x}Ca_xV_3O_7$ and $Ca_{1-x}Sr_xV_3O_7$, where $J_c = J_{c1} = J_{c2}$.

angle would be responsible for the suppression of the magnetic transition temperature. The V1–O3–V1 angle $\sim 120^\circ$ may correspond to the condition $J_\perp \simeq 0$, judging from the results shown in figure 3.

The parameters obtained here are similar to those from the quantum Monte Carlo (QMC) simulation [7], although our $J_c$ is rather large. The disagreement between the experimental and QMC results was attributed to the increase of the relative errors of QMC simulation due to large cancellation effects for the exchange couplings. However, the $\chi$-values obtained in terms of HTSE with the use of previous parameters agree well with those from QMC at temperatures above 100 K. This indicates that the larger antiferromagnetic coupling of $J_c$ is necessary in order to explain results at high temperatures. Our consideration is not consistent with the previous result that $SrV_3O_7$ is regarded as a one-dimensional-like system [25]. This discrepancy may be attributed to the previous method of the analysis that is based on the net change in the orbital energy.

### *3.4. Spin-flop*

From the molecular field theory, the critical magnetic field at which the spin-flop transition occurs, $H_{sf}$, satisfies the following condition:

$$\Delta = \tfrac{1}{2}(\chi_\perp - \chi_\parallel)H_{sf}^2 < \tfrac{1}{2}\chi_\perp H_{sf}^2, \tag{7}$$

where $\chi_\perp$ and $\chi_\parallel$ are the susceptibilities for $H > H_{sf}$ and $H < H_{sf}$, respectively, on the condition that $\boldsymbol{H}$ is applied parallel to $\boldsymbol{S}$, and $\Delta$ is the magnetic anisotropy energy. One can find from figure 4(b) that $\chi_\perp = 7.5\times10^{-4}$ emu (mol V)$^{-1}$ ($9.0 \times 10^{-4}$ emu (mol V)$^{-1}$) and $H_{sf} < 2$ T (2.5 T) for $CaV_3O_7$ ($SrV_3O_7$). Thus, we obtain that $\Delta < 1.8 \times 10^{-3}$ K ($3.4 \times 10^{-3}$ K). The order can be explained by an order of anisotropic superexchange coupling $\sim O((2-g)^2 J_c)$. This means the anisotropy is very small.

Considering the spin-flop on the model of $J_c \gg |J_{e1}|, |J_{e2}|$, the moment arising by breaking the antiferromagnetic correlation between one-dimensional chains with $J_c$ may be important. In this case, $\chi_\perp$ is given by

$$\chi_\perp = \frac{C}{6(J_{e1} - J_{e2})}. \tag{8}$$

The comparison between equation (8) and the experimental results leads to $J_{e1} - J_{e2} = 81$ K (66 K), which is fairly consistent with the HTSE results. Here, it should be noted that the directions of magnetic moments for the stripe phases in $CaV_3O_7$ and $SrV_3O_7$ are different as described in section 1. This suggests that a magnetic anisotropy different from that of the $g$-factor also exists in this system. The nearly field-independent susceptibility of $Ca_{0.7}Sr_{0.3}V_3O_7$, whose value is between those of $SrV_3O_7$ at low and high fields, suggests that the spin-flop has already taken place at a very low field and that the magnetic anisotropy is significantly reduced in this compound.

## 4. Conclusions

For the two-dimensional $S = \frac{1}{2}$ system $MV_3O_7$, where M = $Cd_{1-x}Ca_x$ and $Ca_{1-x}Sr_x$, the crystal structures are determined precisely and the magnetic properties are investigated in detail through the analysis of HTSE. The exchange couplings sharing oxygen corners for the paths of V1–O–V2, $J_{c1}$ and $J_{c2}$, are antiferromagnetic and they are larger than those sharing oxygen edges for the paths of V1–O–V1 ($J_{e1}$) and V1–O–V2 ($J_{e2}$). While $J_{e2}$ is always ferromagnetic, $J_{e1}$ changes from ferromagnetic to antiferromagnetic with an increase of ionic radii of M. No frustration exists in the spin network when $J_{e1}$ is antiferromagnetic and $J_{e2}$ is ferromagnetic, so the appearance of the transition to the stripe phase for $CaV_3O_7$ and $SrV_3O_7$ is understood naturally. For $CdV_3O_7$, $J_{e1} < 0$ and $|J_{e2}| \gg |J_{e1}|$ are fulfilled, so the frustration should not be effective. The absence of magnetic transition may be attributed to the reduction of the coupling between the $V_3O_7$ layers, which may be consistent with the crystal structure.

For the V ions sharing the edge of the basal plane, there exist the V–V direct exchange coupling and the 90° V–O–V superexchange coupling. The former may be antiferromagnetic and it increases with the decrease of the V–V distance. On the other hand, the latter is probably ferromagnetic from a qualitative rule [35]. On the basis of the bond-lengths and bond-angles of $CdV_3O_7$, $CaV_3O_7$ and $Ca_{0.55}Sr_{0.45}V_3O_7$ listed in table 3, it is found that the decrease of V1(i)–V1(ii) with the increase of the ionic radii of M is more significant than the increase of V1(i)–V2(iii). This suggests that the exchange coupling of V1–V1 ($J_{e1}$) becomes more antiferromagnetic and that of V1–V2 ($J_{e2}$) remains ferromagnetic. This is consistent with the results estimated from HTSE. For the coupling between V ions sharing corners ($J_c$), the angles of V1(i)–O1(i)–V2(vii) and V1(i)–O2(i)–V2(i) both increase on increasing the ionic radii of M. This tendency also supports the HTSE results.

## Acknowledgments

We would like to thank Y Uchida for the use of the SQUID susceptometer, and A Ohyama for help with the HTSE calculation.

## Appendix. Application of HTSE to the $MV_3O_7$ system

HTSE is the expression expanded with $\frac{J}{T}$ and it is generally valid with $T \gg J$ such that the higher terms are negligible. The higher terms become effective with decreasing temperature,

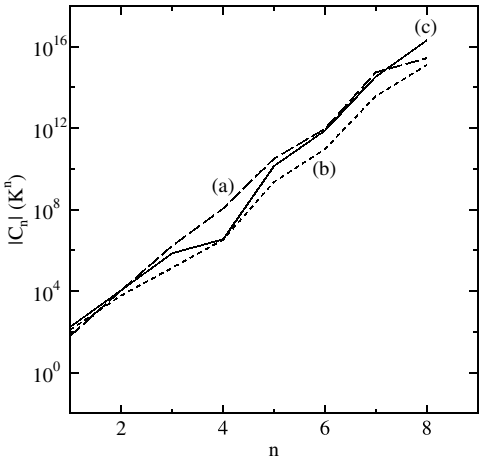


**Figure A.1.** The relation between the coefficient of $(\frac{1}{T})^n$, $|C_n|$, and $n$.

**Table A.1.** The parameter set $J_{e1}$, $J_{e2}$ and $J_c$ (K) that roughly reproduces the susceptibility data of $MV_3O_7$, where a negative value indicates a ferromagnetic coupling.

| | Case (a) | Case (b) | Case (c) |
|---|---|---|---|
| $J_{e1}$ | −12.5 | 45.2 | 40.0 |
| $J_{e2}$ | −164.1 | −19.0 | −23.8 |
| $J_c$ | 184.9 | 178.0 | 256.4 |

and all of the terms are necessary for the region of $T < J$. Generally, the spin susceptibility $\chi_s$ is expressed as

$$\chi_s = \frac{1}{J} f\left(\frac{T}{J}\right), \tag{A.1}$$

where $f(x)$ is some function. The lower temperature limit $T_{min}$ for the application of HTSE of up to the eighth order is determined with $J$, because $\chi$ is only a function of $\frac{T}{J}$.

As described in the text, four types of exchange coupling exist in $MV_3O_7$. In this case, we have to consider how the effective exchange coupling $J_{eff}$ is defined. As a trial, the parameter set listed in table A.1, which roughly reproduces the susceptibility of $MV_3O_7$, is considered. The absolute values of the coefficient of $1/T^n$, $|C_n|$, are found to vary exponentially as a function of $n$ (figure A.1), which indicates that the term of $1/T^n$ may be expressed as

$$A\left(\frac{B}{T}\right)^n, \tag{A.2}$$

where $A$ and $B$ are constants. This means that $T_{min}$ exists for the application of HTSE in $MV_3O_7$. Thus, $J_{eff}$ is assumed to be $B$.

For the HTSE analysis of experimental data, $T_{min}$ is assumed to range from $2.2J_{eff}$ to $2.3J_{eff}$.

## References

[1] Taniguchi S, Nishikawa T, Yasui Y, Kobayashi Y, Sato M, Nishioka T, Kontani M and Sano K 1995 *J. Phys. Soc. Japan* **64** 2758

[2] Kodama K *et al* 1997 *J. Phys. Soc. Japan* **66** 793

[3] Onoda M and Nishiguchi N 1996 *J. Solid State Chem.* **127** 359
[4] Onoda M and Ohyama A 1998 *J. Phys.: Condens. Matter* **10** 1229
[5] Millet P, Satto C, Bonvoisin J, Normand B, Penc K, Albrecht M and Mila F 1998 *Phys. Rev.* B **57** 5005
[6] Miyahara S, Troyer M, Johnston D C and Ueda K 1998 *J. Phys. Soc. Japan* **67** 3918
[7] Korotin M A, Elfimov I S, Anisimov V I, Troyer M and Khomskii D I 1999 *Phys. Rev. Lett.* **83** 1387
[8] Korotin M A, Anisimov V I, Saha-Dasgupta T and Dasgupta I 2000 *J. Phys.: Condens. Matter* **12** 113
[9] Konstantinović M J, Popović Z V, Isobe M and Ueda Y 2000 *Phys. Rev.* B **61** 15 185
[10] Onoda M and Kagami T 1999 *J. Phys.: Condens. Matter* **11** 3475
[11] Miyata T, Miura I, Onoda M and Nagasawa H 1993 *48th Annu. Mtg Phys. Soc. Japan* part 3, abstracts (Tokyo: Physical Society of Japan) p 23 (in Japanese)
[12] Ohyama A 1998 *Master's Thesis* University of Tsukuba (in Japanese)
[13] Isobe M and Ueda Y 1996 *J. Phys. Soc. Japan* **65** 3142
[14] Mur J and Darriet J 1985 *C. R. Acad. Sci., Paris* **13** 599
[15] Kanada M, Harashina H, Tanaka S, Fukamachi T, Kobayashi Y and Sato M 1998 *J. Phys. Soc. Japan* **67** 2904
[16] Onoda M and Nishiguchi N 1999 *J. Phys.: Condens. Matter* **11** 749
[17] Bouloux J C and Galy J 1973 *Acta Crystallogr.* B **29** 269
[18] Shannon R D 1976 *Acta Crystallogr.* A **32** 751
[19] Miyata T 1993 *Master's Thesis* University of Tsukuba (in Japanese)
[20] Taniguchi S, Kobayashi Y, Kasai M, Kodama K and Sato M 1997 *J. Phys. Soc. Japan* **66** 3660
[21] Liu G and Greedan J E 1993 *J. Solid State Chem.* **103** 139
[22] Harashina H, Kodama K, Shamoto S, Taniguchi S, Nishikawa T, Sato M, Kakurai K and Nishi M 1996 *J. Phys. Soc. Japan* **65** 1570
[23] Kontani H, Zhitomirsky M E and Ueda K 1996 *J. Phys. Soc. Japan* **65** 1566
[24] Takeo Y *et al* 1999 *J. Phys. Chem. Solids* **60** 1153
[25] Whangbo M-H, Koo H-J and Lee K-S 2000 *Solid State Commun.* **114** 27
[26] Onoda M, Ohta H and Nagasawa H 1991 *Solid State Commun.* **79** 281
[27] Hai-Fu F 1991 *SAPI91: Structure Analysis Programs with Intelligent Control* (Tokyo: Rigaku)
[28] Cromer D T and Waber J T 1974 *International Tables for X-Ray Crystallography* vol 4, ed J A Ibers and W C Hamilton (Birmingham: Kynoch) section 2
[29] Creagh D C and McAuley W J 1992 *International Tables for Crystallography* vol C, ed A J C Wilson (Boston, MA: Kluwer)
[30] teXsan 1992 *Crystal Structure Analysis Package* (The Woodlands, TX: Molecular Structure Corporation)
[31] Zachariasen W H 1978 *J. Less-Common Met.* **62** 1
[32] Marshall W 1959 *Proc. R. Soc.* A **232** 48
[33] Lieb E and Mattis D 1962 *J. Math. Phys.* **3** 749
[34] See, for example, Yamamoto S, Fukui T, Maisinger K and Schollwöck U 1998 *J. Phys.: Condens. Matter* **10** 11 033
[35] See, for example, Goodenough J B 1963 *Magnetism and the Chemical Bond* (New York: Interscience) ch 3